The Journal of Experimental Biology 200, 3165–3183 (1997)
Printed in Great Britain © The Company of Biologists Limited 1997
JEB1288

FLOW AND FLEXIBILITY

II. THE ROLES OF SIZE AND SHAPE IN DETERMINING WAVE FORCES ON THE BULL KELP *NEREOCYSTIS LUETKEANA*

MARK W. DENNY[1,*], BRIAN P. GAYLORD[1] AND EDWIN A. COWEN[2]

[1]*Hopkins Marine Station of Stanford University, Department of Biological Sciences, Pacific Grove, CA 93950, USA* and [2]*Civil Engineering Department, Stanford University, Pacific Grove, CA 93950, USA*

Accepted 2 October 1997

Summary

Giant kelps (which may reach lengths of 45 m) are a prominent exception to the general rule that wave-swept organisms are small. The ability of these kelps to maintain their large size in the presence of ocean waves has been attributed to their extreme flexibility and the concomitant tendency to 'go with the flow', a tendency that reduces the hydrodynamic forces imposed on the plant. However, the flexibility of giant kelps carries with it the potential for the organism to apply an inertial load to its own structure if the blade mass reaches the end of its tether. Here, we examine the complex trade-off between flexibility and inertial loading using a simple computational model of the bull kelp *Nereocystis luetkeana*. In field and laboratory tests, the model accurately predicts the forces and motions imposed on flexible structures in wave-induced flows. Subsequent predictions from the model suggest that mature *N. luetkeana* can indeed benefit from moving with the flow, but that the forces imposed on juveniles are actually increased by the plant's flexibility. Furthermore, the benefit accrued from going with the flow is sensitive to the shape of the plant. If the bull kelp were to grow while maintaining a juvenile shape, the stress placed on its stipe would be drastically increased by dynamic loading, and these inappropriately shaped plants would be subjected to a high risk of breakage. For certain combinations of wave height, wave period and stipe length, the increased stress in hypothetical 'small'-shaped plants may be associated with chaotic motion of the blade mass.

Key words: kelp, *Nereocystis luetkeana*, wave forces, hydrodynamic forces.

Introduction

Wave-swept rocky shores support a surprisingly diverse assemblage of organisms that includes members of virtually every animal phylum and both algae and vascular plants. In general, wave-swept organisms are small compared with their subtidal or terrestrial cousins, and it has been proposed that hydrodynamic forces can play an important role in limiting the size of wave-swept plants and animals (Denny *et al.* 1985; Denny, 1988; Carrington, 1990; Gaylord *et al.* 1994). As an organism grows, the forces placed on it by moving water typically increase at a faster rate than the strength of the organism, and the risk of breakage or dislodgment therefore increases with increasing body size. This scaling of risk sets an absolute upper size to any particular organism (governed by the severity of the wave environment) and may set an optimum size at which reproductive output is maximized.

Large kelps appear to be exceptions to these rules. Species such as the giant kelp *Macrocystis pyrifera* and the bull kelp *Nereocystis luetkeana* grow to lengths of 20–45 m (more than 10 times that typical of intertidal algae) and have frond areas measured in tens of square meters. It has been proposed that for these giant kelps large size is advantageous (e.g. Koehl and Wainwright, 1977; Koehl, 1984, 1986; Denny, 1988): if the plant is large enough and flexible enough, it can simply 'go with the flow' as waves pass by, reducing the relative velocity and acceleration between the plant and the surrounding water and, thereby, reducing the imposed hydrodynamic forces. In this scenario, the giant kelps are thought to have grown past a physical bottleneck in the evolution of size and have come upon a pattern of growth in which 'bigger' may truly be 'better'. Indeed, on many wave-swept shores, giant kelps are the dominant competitors for space on the subtidal substratum (Foster and Schiel, 1985).

As compelling as this scenario may be, it is unlikely to be the full story. Large kelps have a substantial mass of blades (the frond mass of a mature bull kelp may weigh 20 kg) that is tethered to the substratum by the plant's stipe. As the distal portion of the plant moves with the surrounding fluid, the plant's blade mass may achieve a substantial velocity and

*e-mail: mwdenny@leland.stanford.edu

thereby a substantial momentum. If while moving at this velocity the blades come to the end of their tether, the abrupt change in momentum can apply a large tension to the stipe. Thus, the ability to move with the flow carries with it the potential for the plant to apply an inertial load to its own structure.

The consequences of this type of dynamic loading on giant kelps have not been explored in detail. Friedland and Denny (1995) examined the forces imposed by surf-zone flows on the feather boa kelp *Egregia menziesii* using a numerical model, but these plants are small compared with the giant kelps (typically 2–3 m long for intertidal *E. menziesii*), and the flows to which they are subjected are substantially different from those found subtidally where giant kelps grow. Utter and Denny (1996) used a similar numerical model to predict the long-term force imposed on the giant kelp *M. pyrifera* and compared these predictions with the maximum forces measured in the field. No attempt was made, however, to compare predicted and measured forces on a wave-by-wave basis, nor to explore how the stresses placed on these plants vary through ontogeny. The dynamics of *M. pyrifera* is also complicated by the fact that many stipes emerge from a single holdfast, and it appears likely that it is the interaction among stipes that controls the maximum hydrodynamic force imposed on the plant. Dayton *et al.* (1984) and Seymour *et al.* (1989) report extensive measurements of the survivorship of *M. pyrifera* and its correlation with wave conditions, but they do not address the mechanics of giant kelps in flow.

In the present study, we explore the dynamics of the bull kelp *Nereocystis luetkeana* (Mertens), a member of the Laminariales and a close phylogenetic cousin of *M. pyrifera* and *Pelagophycus porra*, the other giant kelps of the west coast of North America. *N. luetkeana* typically occurs subtidally at depths of 10–17 m (although it may occasionally be found at shallower depths), with a latitudinal range from Alaska to central California (Abbott and Hollenberg, 1976). The plant consists of a holdfast, a narrow flexible stipe (which may reach 25 m in length), a bulbous gas-filled float (the pneumatocyst) and 30–64 blades, each of which may exceed 4 m in length (Fig. 1). The upper part of the stipe is hollow, and this cavity is continuous with that of the pneumatocyst. *N. luetkeana* is an annual, appearing first in late winter or early spring, growing to full height by early summer, and reproducing and becoming senescent in late summer and autumn. In central California, *N. luetkeana* is generally found only on very exposed shores where it supplants *M. pyrifera* (Dayton *et al.* 1984), but in Washington state, British Columbia and Alaska, *N. luetkeana* can also be found in more protected habitats exposed to tidal currents (e.g. Koehl and Wainwright, 1977; Johnson and Koehl, 1994).

Koehl and Wainwright (1977) and Johnson and Koehl (1994) have examined in some detail the mechanics of the materials from which *N. luetkeana* stipes are constructed and the shapes in which this species grows when exposed to various flow regimes. However, their calculations of the forces placed on the plant are based on the assumption that flow is unidirectional and steady. Thus, the question of how the dynamics of plant motion affects the forces placed on *N. luetkeana* has not been addressed.

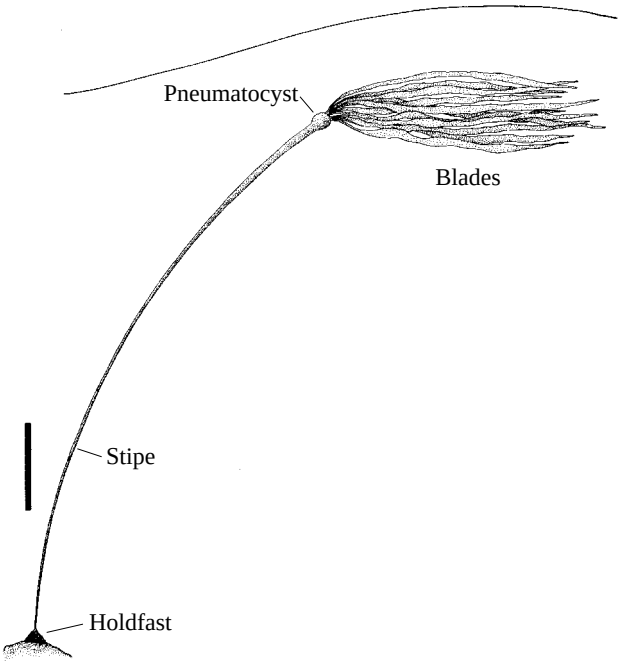

Fig. 1. *Nereocystis luetkeana.* The scale bar is 1 m long.

Our study consists of four parts. A simple mathematical model is constructed that we believe incorporates the most important aspects of the dynamics of giant kelps. Measurements of the size and shape of actual *N. luetkeana* then allow us to tailor this model to reflect the dimensions of the kelp as it grows. The predictions of the model are compared empirically with the forces encountered by plants in the field and with the motions of model plants in the laboratory. The validated model is then used to explore the role of size in the forces placed on this giant kelp and the consequences of allometric growth.

A simple numerical model of *Nereocystis* mechanics

The model is similar in principle to that developed by Friedland and Denny (1995) for *E. menziesii* and Utter and Denny (1996) for *M. pyrifera* (Fig. 2). The distributed forces acting on an entire *N. luetkeana* plant, as well as the plant's entire mass, are assumed to act at a single point element. The point element is tethered to the substratum by a flexible, elastic rope that acts as a model of the plant's stipe. Waves propagate across the water's surface, moving the water beneath them, and relative motion between the point element and the surrounding water imposes drag and hydrodynamic accelerational forces on the plant. These fluid-dynamic forces (plus the plant's net buoyancy) are resisted by the tension in the 'stipe', and any imbalance among these forces results in the acceleration of the point element. Numerical integration of this acceleration through time provides a time series of the velocity and location

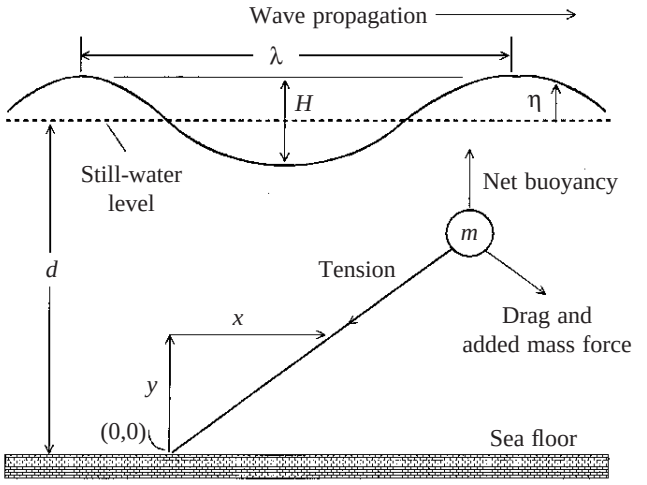

Fig. 2. A schematic representation of the numerical model of kelp dynamics. For further details, see the text. *d*, water column depth; *H*, wave height; η, vertical deviation from still-water level; *m*, plant mass; *x*, *y*, horizontal and vertical coordinate axes, respectively; λ, wavelength.

of the point element and of the tension in the 'stipe'. The characteristics of this time series can then be examined as a function of wave height and period, water depth, the shape of the plant and the length of the tether to explore the dynamic mechanical design of *N. luetkeana*.

The water column

The seabed is assumed to be planar and horizontal, and the water column has a still-water depth, *d* (Fig. 2). A stationary Cartesian coordinate system is used, with its origin fixed at the seabed. The water's surface is at $y=d+\eta$, where η is the vertical deviation from still-water level and is a function of both *x* and time, *t*. All motion of the plant and water is assumed to occur in the *x*,*y* plane. The basal end of the model plant's stipe is fixed to the origin, and its distal end is attached to the point element at position (*x*,*y*).

At any time, the point element has velocity $\mathbf{u_k}$ and acceleration $\mathbf{a_k}$. At the same time, the water at (*x*,*y*) has velocity **u** and acceleration **a**. The relative velocity between the water and the point element is $\mathbf{u_r}=\mathbf{u}-\mathbf{u_k}$ and the relative acceleration is $\mathbf{a_r}=d\mathbf{u_r}/dt=\mathbf{a}-\mathbf{a_k}$. All variables shown in bold type are vectors, and a list of variables is provided in Table 1.

Forces

As noted above, the point element has a mass equal to the combined stipe and blade mass of the plant being modeled and is subjected to all the forces imposed on the plant. The forces are listed below.

Net buoyancy

The net submerged buoyant force, $\mathbf{F_{sb}}$, acting on the element is the difference between the plant's hydrostatic buoyancy and its weight. The positive net buoyancy of an actual *N. luetkeana*

Table 1. *A list of symbols used*

Symbol	Definition	Equation of first use
A	Maximal projected area	2
A_{xs}	Cross-sectional area of stipe	5
$\mathbf{a}$	Acceleration of the water	3
$\mathbf{a_k}$	Acceleration of the point element	4
$\mathbf{a_r}$	Relative acceleration	4
a_x	Horizontal water acceleration	15
a_y	Vertical water acceleration	16
C_a	Added mass coefficient	4
D	Table-tennis ball diameter	
d	Water column depth	1
e_f	Fractional error	19
E	Stiffness of stipe material	5
$\mathbf{F_{am}}$	Added mass force	4
$\mathbf{F_b}$	Net buoyant force	1
$\mathbf{F_d}$	Drag	2
F_{obs}	Observed maximal force	19
F_{pred}	Predicted maximal force	19
$\mathbf{F_r}$	Restoring force	7
$\mathbf{F_{sb}}$	Net submerged buoyancy	1
$\mathbf{F_{vb}}$	Virtual buoyancy	3
$\boldsymbol{g}$	Gravitational acceleration	12
H	Wave height	9
H_s	Significant wave height	–
k	Wave number	9
L	Stipe length	5
ΔL	Change in stipe length	20
m	Plant mass	8
R	Stress ratio	22
r_e	Equivalent radius	9
r_s	Equivalent stipe radius	–
SEE	Standard error of the regression estimate	–
S_d	Shape coefficient of drag	2
$\mathbf{T}$	Tension	5
t	Time	8
$\mathbf{u}$	Velocity of the water	–
$\mathbf{u_k}$	Velocity of the point element	8
u_{max}	Maximal relative velocity in a wave cycle	–
$\mathbf{u_r}$	Relative velocity	2
u_r	Magnitude of the relative velocity	2
u_x	Horizontal water velocity	13
u_y	Vertical water velocity	7
V	Plant volume	3
x	Horizontal coordinate axis	5
y	Vertical coordinate axis	1
y_{mt}	y at time of maximal tension	–
α	Allometric coefficient	17
β	Allometric exponent	17
γ	Velocity exponent of drag	2
η	Vertical deviation from still-water level	1
λ	Wavelength	10
ρ	Density of sea water	2
θ_t	Angle between stipe and horizontal	–
σ_{act}	Actual tensile stress	22
σ_{stat}	Static tensile stress	22
τ	Wave period	11
ω	Radian wave frequency	9

Symbols in bold type are vectors.

is due to the low density of its gas-filled pneumatocyst, and the size of this structure leads to a minor complication in the model when the point element encounters the surface. If the pneumatocyst were to behave as a true point element, its net buoyancy would be constant until it reached the surface, and above the surface it would be subjected to a downward force equal to the weight of the entire plant. However, this discontinuity in vertical force is not a sufficiently accurate model of an actual kelp. Instead, we suppose that the net buoyant force $\mathbf{F_b}$ acting on the point element decreases gradually as the element moves above the water's surface, as it would when an actual pneumatocyst protrudes above the water:

$$\mathbf{F_b} = \mathbf{F_{sb}}\left(1-\frac{y-[d+\eta(x)]}{0.75}\right), \quad y > d+\eta(x)\,.$$

$$\mathbf{F_b} = \mathbf{F_{sb}} \quad y \leqslant d+\eta(x)\,. \tag{1}$$

Thus, the net buoyancy decreases linearly to zero when the top 0.75 m of the plant is above the water's surface. The factor of 0.75 m is set by field observations of the length of stipe lying recumbent on the water's surface at low tide when the stipe is longer than the water's depth.

Drag

Relative motion between the point element and the surrounding water imposes a drag $\mathbf{F_d}$ in the direction of relative velocity:

$$\mathbf{F_d} = \tfrac{1}{2}\rho \mathbf{u_r} u_r^{\gamma-1} A S_d\,. \tag{2}$$

Here, ρ is the density of sea water (1025 kg m^{-3}), A is the maximum projected blade area of the plant, S_d is a shape coefficient of drag and γ is the velocity exponent. Note that S_d has the dimensions m$^{2-\gamma}$s$^{\gamma-2}$. For a complete discussion of this equation, see Gaylord *et al.* (1994) or Denny (1995).

Utter and Denny (1996) measured a value of 1.6 for the velocity exponent of *M. pyrifera*, and this value is used here. Measurements conducted by Johnson and Koehl (1994) suggest that, for the streamlined morphs of *N. luetkeana* in Washington State (similar to those used in the present study), S_d is approximately 0.016, and this value is used here.

Virtual buoyancy

When the water at (x,y) accelerates relative to the substratum, the point element is subjected to a decreasing pressure gradient in the direction of acceleration. As a result, a virtual buoyancy $\mathbf{F_{vb}}$ acts on the point element in the direction of the water's acceleration:

$$\mathbf{F_{vb}} \approx \rho V \mathbf{a}\,, \tag{3}$$

where V is the volume of fluid displaced by the plant (Batchelor, 1967).

Added mass force

If, in addition to accelerating relative to the seabed, the water at (x,y) accelerates relative to the point element, an additional force is imposed in the direction of relative acceleration. This added mass force $\mathbf{F_{am}}$ is:

$$\mathbf{F_{am}} \approx \rho C_a V \mathbf{a_r} = \rho C_a V \mathbf{a} - \rho C_a V \mathbf{a_k}\,. \tag{4}$$

Here, C_a is the dimensionless added mass coefficient (Batchelor, 1967). Gaylord *et al.* (1994) measured added mass coefficients for a variety of wave-swept algae and found them to vary between 1.6 and 6.7. Utter and Denny (1996) found that a value of 3.0 best fitted reality in their simulation of *M. pyrifera*, and this value is used here.

Note that $\mathbf{F_{vb}}$ and $\mathbf{F_{am}}$ as formulated here are approximations in that they do not include terms dealing with the convective acceleration of the fluid (for a discussion of these terms, see Sarpkaya and Isaacson, 1981; Miloh, 1994). Trial calculations including the convective terms showed that they have a negligible effect in this system and, for simplicity, they have not been included in the final model.

Tension

The tether attaching the point element to the holdfast is modeled as an elastic, massless rope. That is, the tether exerts a tensile force $\mathbf{T}$ on the element when it is stretched beyond its resting length, L, but exerts no force when the point element is closer to the origin than the unstretched length of the tether:

$$\mathbf{T} = EA_{xs}\left[\frac{\sqrt{(x^2+y^2)}-L}{L}\right], \qquad \sqrt{(x^2+y^2)} > L\,,$$

$$\mathbf{T} = 0 \qquad \sqrt{(x^2+y^2)} \leq L\,. \tag{5}$$

Here, E is the stiffness of the stipe material (in Pa) and A_{xs} is the nominal cross-sectional area of the stipe (in m^2). The tensile force is directed towards the origin along the rope, i.e. at an angle θ_t=arctan(y/x) to the horizontal. For *N. luetkeana*, which grow in areas exposed to substantial water motion, Johnson and Koehl (1994) found that the stiffness of the stipe varied with extension from 16–18 MPa at low extensions to 8 MPa at high extensions. An extension-independent intermediate value of 12 MPa is used here. Johnson and Koehl (1994) note that the mechanical properties of *N. luetkeana* stipe material seem to be independent of stipe length.

Contact of the point element with the seabed

When the stipe is short and the waves are high, it is possible that the point element may come into contact with the seabed. Because there is nothing inherent in the force balance between the tether and the forces acting on the plant's mass that prohibits the point element from (unrealistically) moving to negative values of y, an additional constraint must be added to the model. An equivalent radius r_e is assigned to the point element from a consideration of the plant's volume:

$$r_e = \left(\frac{3V}{4\pi}\right)^{1/3}. \tag{6}$$

If the point element moves to $y<r_e$, an arbitrarily formulated,

vertical, damped, elastic restoring force $\mathbf{F_r}$ is placed upon it, analogous to a ball impacting on a floor:

$$\mathbf{F_r} = \left[2\log\left(\frac{y}{r_e}\right) - 100u_y|u_y|\right](m + \rho C_a V), \qquad y < r_e,$$

$$\mathbf{F_r} = 0 \qquad y \geq r_e, \tag{7}$$

where u_y is the vertical water velocity and m is plant mass.

Force balance

Any net force acting on the point element causes that element to accelerate at a rate equal to the net force divided by the element's mass. Thus, from Newton's Second Law of motion:

$$\mathbf{a_k} = \frac{d\mathbf{u_k}}{dt} = \frac{\mathbf{F_b} + \mathbf{F_d} + \mathbf{F_{vb}} + \mathbf{F_{am}} + \mathbf{T} + \mathbf{F_r}}{m}. \tag{8}$$

This equation can be integrated numerically through time to provide a time series of both the velocity and location of the point element. From the time series of x,y values, a corresponding time series of tensions in the modeled stipe can be calculated using equation 5. A fourth-order Runge–Kutta algorithm was used for these integrations (Dahlquist and Björck, 1974), with two implementations. For most experiments, an adaptive time step was used (Press *et al.* 1992). The ability of the program to adjust the time step during integration allows the program to maintain a nearly constant accuracy throughout the calculation, even when the acceleration of the point element is abrupt. The disadvantage of the adaptive time step is that values of $\mathbf{u_k}$, x, y and $\mathbf{T}$ are not calculated at equally spaced intervals, which can be problematic for certain subsequent calculations (e.g. of power spectra and Lyapunov exponents). When it is necessary that velocity, position or tension be recorded at specific intervals, a fixed, small time step is used.

Wave-induced water motion.

The motion of water beneath ocean waves is modeled using linear wave theory (see, for example, Kinsman, 1965; Denny, 1988). The deviation of the water's surface from the still-water level, η, at position x and time t is:

$$\eta = \frac{H}{2}\cos(kx - \omega t). \tag{9}$$

Here, H is the wave height, the vertical distance from trough to crest (Fig. 2). The wave number, k, is:

$$k = \frac{2\pi}{\lambda}, \tag{10}$$

and the radian wave frequency, ω, is:

$$\omega = \frac{2\pi}{\tau}, \tag{11}$$

where τ is the wave's period. Wavelength, λ, is a function of wave period and water-column depth and can be estimated from a relationship derived by Eckart (1952):

$$\lambda \approx \frac{g\tau^2}{2\pi}\sqrt{\tanh\left(\frac{4\pi^2 d}{\tau^2 g}\right)}. \tag{12}$$

At position (x,y), the horizontal water velocity u_x and vertical water velocity u_y (both measured relative to the stationary substratum) are:

$$u_x = \frac{\pi H}{\tau}\cos(kx - \omega t)\frac{\cosh(ky)}{\sinh(kd)}, \tag{13}$$

$$u_y = \frac{\pi H}{\tau}\sin(kx - \omega t)\frac{\sinh(ky)}{\sinh(kd)}. \tag{14}$$

The horizontal and vertical water accelerations are:

$$a_x = \frac{\omega\pi H}{\tau}\sin(kx - \omega t)\frac{\cosh(ky)}{\sinh(kd)}, \tag{15}$$

$$a_y = -\frac{\omega\pi H}{\tau}\cos(kx - \omega t)\frac{\sinh(ky)}{\sinh(kd)}. \tag{16}$$

The overall velocity is the vector sum of u_x and u_y.

Materials and methods

Morphology

In July and September 1994, 27 *N. luetkeana* (Mertens) were collected using SCUBA from Carmel Point (Carmel-by-the-Sea, California) and an additional 28 individuals from Salt Point (near the Bodega Marine Laboratory, Bodega, California). Plants of the widest possible range of sizes were sampled haphazardly and immediately returned to the laboratory. For each plant, the following characteristics were measured.

Overall plant mass, m

Each large plant was trimmed of it holdfast, placed in a preweighed mesh bag and suspended from a calibrated spring scale. The net mass of the plant was determined to the nearest 0.05 kg. Small plants (<1.2 kg) were weighed to the nearest 0.01 g on a laboratory balance.

Maximum projected blade area, A

Blades were outlined with pencil on large sheets of paper, and the outlines were cut out and weighed. Area was then calculated by comparing the mass of the cut-outs with the mass of a known area of paper. Blades were narrow and lacked undulations on their edges, and were therefore similar to the current-swept morphology of Johnson and Koehl (1994).

Stipe length, L

The length of the stipe (from the top of the holdfast to the top of the pneumatocyst) was measured to the nearest centimeter using a tape measure.

Minimum stipe cross-sectional area, A_{xs}

The stipe was measured at its narrowest point, typically just

above the holdfast. The maximum diameter at this point was measured as well as the diameter at right angles to the maximum. The minimal cross-sectional area was determined by treating the stipe's cross section as an ellipse and calculating the area from the measured diameters. From the area, an equivalent stipe radius r_s can be calculated:

$$r_s = \sqrt{(A_{xs}/\pi)}\ . \tag{17}$$

Net buoyancy

A weighted mesh bag was suspended by a string from an electronic scale so that the bag was immersed in sea water, and the net weight of the bag was noted. A plant was then inserted into the bag, and the new weight measured. The difference in weight with and without the plant is the plant's net submerged buoyancy $\mathbf{F_{sb}}$. Net buoyancy was measured to the nearest 0.001 N in small plants and to the nearest 0.01 N in large plants.

The allometric relationships between stipe length and overall mass, frond area, stipe cross-sectional area and buoyancy were determined from an ordinary least-squares regression of the natural logarithm of stipe length against the natural logarithm of the character of interest. The use of the logarithmic transformation was necessary owing to heteroscedasticity in the data (Zar, 1974). The resulting relationships are of the form:

$$\text{trait of interest} = \alpha L^{\beta}, \tag{18}$$

in which the value of α as initially determined from the regression has been multiplied by $e^{SEE^2/2}$, a factor used to correct for the bias introduced by the $\log_e$ transformation (Beauchamp and Olson, 1973; Sprugel, 1983). *SEE* is the standard error of the regression estimate.

N. luetkeana plants typically increase in both length and blade area until the pneumatocyst reaches the water's surface. At this point, the stipe ceases to lengthen, although the blades continue to increase in area (Duncan, 1973; Duncan and Foreman, 1980). As a result of this shift in the pattern of growth, the length of the stipe becomes a very poor predictor of blade area and plant mass for those plants that have reached the surface, and plants with stipes equal to or greater than the local depth were excluded from the prediction of blade area and overall mass. Mature plants typically have a blade area and blade mass 2–4 times that predicted by the allometric equation.

The precise manner in which *N. luetkeana* plants adjust their morphology has been shown to depend on the local hydrodynamic environment (Johnson and Koehl, 1994), and the measurements obtained in the present study may therefore apply only to plants inhabiting exposed sites in central California.

Field measurements

To provide a test of the ability of our numerical model to predict the actual forces on *N. luetkeana*, measurements of the tensile forces imposed on *N. luetkeana* in the field were conducted using the apparatus shown in Fig. 3. The stipe of a mature *N. luetkeana* was attached *via* a short length of nylon rope to a stiff cantilever-type strain-gauge force transducer that was mounted in turn on a heavily weighted aluminum plate that rested horizontally on the seabed. The voltage output from the transducer (proportional to the tension in the stipe) was amplified and recorded at 20 Hz by a digital datalogger (Tattletale model 5F) mounted in a waterproof housing. To provide an estimate of the instantaneous surface elevation above the apparatus, simultaneous 20 Hz measurements of hydrostatic pressure were recorded from a transducer (Omega PX176A) mounted in the same housing as the datalogger. The morphological characteristics of the test plant (measured subsequent to the field experiment) are given in Table 2.

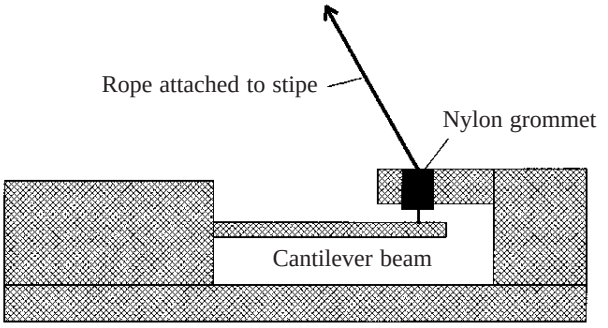

Fig. 3. A schematic representation of the force transducer used to measure the tension on a kelp stipe in the field. Strain gauges glued to the beam transduce the beam's deflection to a voltage that is recorded by the datalogger. The low-friction grommet ensures that the transducer senses the tension in the stipe regardless of the angle at which tension is applied.

The device was deployed off the shore at Hopkins Marine Station, Pacific Grove, California, and tension and pressure were recorded for 30 min on 23 September 1995. The surf conditions during the deployment were characterized by a significant wave height, H_s, of 0.8 m. H_s is the mean height of the highest one-third of waves, a statistical index of the 'waviness' of the ocean (Longuet-Higgins, 1952). Swell with a period of approximately 16 s was combined with a high-amplitude surfbeat with a peak period of approximately 200 s. Although these wave conditions are benign compared with those present during storms, they are near the extreme at which the device can be safely deployed by SCUBA divers.

For ease of analysis, the lengthy records of tension and hydrostatic pressure were broken into eight consecutive intervals of 4096 data points (approximately 204 s). For each

Table 2. *The morphological characteristics of the* Nereocystis luetkeana *plant tested in the field*

Length, L	6.57 m
Mass, m	8.00 kg
Net buoyancy, F_{sb}	12.51 N
Equivalent minimum stipe radius, r_s	5.8×10^{-3} m
Blade area, A	4.159 m^2

interval, our numerical model was used to predict the tension acting on the stipe of the experimental plant. This prediction was made by incorporating into the numerical model the actual dimensions and buoyancy of the plant (Table 2) and the time course of the ocean's surface elevation.

In the field, wave height and period varied through time, and the actual motion of the water was simulated by the superposition of waves of a range of frequencies with appropriately adjusted amplitudes and phases. To this end, the pressure signal measured at the seabed was used to calculate the temporal variation in surface elevation.

The hydrostatic pressure signal from a surface wave is attenuated by depth by an amount that depends on the frequency (Kinsman, 1965). To counteract this effect, each record of 4096 pressures measured at the seabed was Fourier-transformed, and the Fourier coefficients were corrected to reflect the amplitude at the surface (for a more complete explanation, see Denny, 1988). The first 50 Fourier coefficients were then used to calculate the component waves contributing to the variation in surface elevation. The time series of surface elevations calculated using these Fourier coefficients closely matched that actually recorded.

The water motions corresponding to this pattern of surface elevation were then used by the numerical model to calculate the tension in the stipe. These tensions were in turn compared with the measured stipe tensions for similarity in the mean and standard deviation of forces and for the wave-by-wave error in the estimation of maximal force:

$$e_f = 2\,\frac{F_{obs} - F_{pred}}{F_{obs} + F_{pred}}\ , \qquad (19)$$

where e_f is fractional error, F_{obs} is the measured maximal force and F_{pred} is the predicted maximal force. The first 20 s of each calculated record was excluded from this analysis to ensure that the data were not contaminated by calculations made during the initial equilibration of the numerical model.

Laboratory measurements

Further exploration of the ability of our numerical model to predict the dynamics of *N. luetkeana* was provided by a series of laboratory measurements of the kinematics of small-scale physical models exposed to wave-induced water motions in a wave tank. The models consisted of a small sphere of radius 1.89 cm (a table-tennis ball) tethered to the floor of the wave tank by several parallel lengths of rubber thread. The density of the ball was adjusted either by leaving it full of air (for an overall density of 85.5 kg m^{-3}) or by filling it completely with corn oil, giving the ball an overall density of 952.4 kg m^{-3}. The stiffness of the elastic tether was measured directly by suspending a series of weights from the threads and noting their extension. For the tether of the air-filled ball, tension **T** (in N) is given by:

$$\mathbf{T} = 3.50\Delta L^{0.592}\,, \qquad (20)$$

where ΔL is the extension of the thread (in m) beyond its resting length of 0.51 m. For the tether (consisting of fewer threads) of the oil-filled ball,

$$\mathbf{T} = 0.919\Delta L^{0.447}\,, \qquad (21)$$

and the unstretched length was 0.57 m.

Drag on the table-tennis balls was calculated using γ=2.0 and values of S_d and C_a were estimated from measurements made by Sarpkaya (1975). For the size of ball and frequency of oscillation used in these tests, these coefficients are sensitive to the distance the fluid moves in one wave oscillation relative to the object compared with the object's diameter. This ratio is the period parameter $u_{max}\tau/D$. Here, u_{max} is the maximum relative velocity between the ball and the water and D is the ball's diameter. u_{max} was estimated for each experiment using a preliminary numerical model with S_d=0.5 and C_a=0.5. The estimated period parameter for the air-filled ball experiment was 11, for which Sarpkaya (1975) gives an added mass coefficient of 0.25 and a shape coefficient of 0.60. The period parameter for the corn-oil-filled ball experiment was 5, with a corresponding C_a of 0.50 and S_d of 0.45. Subsequent estimates of u_{max} using these revised coefficients did not substantially alter the period parameter.

These physical models were placed one at a time in a wave tank in the Environmental Fluid Mechanics Laboratory at the Civil Engineering Department, Stanford University (Hsu, 1965; Bole and Hsu, 1969). The tank was filled with fresh water (density nominally 1000 kg m^{-3}) to a depth of 0.75 m, and sinusoidal waves of a constant period and height were generated approximately 10 m upstream of the models by a hydraulically driven ram. The model was viewed through a glass window in the side of the tank, and the motions of the ball in the vertical x,y plane were recorded on video tape at 30 frames s^{-1}. The video camera was placed approximately 4.5 m from the model and equipped with a telescopic lens to minimize the effects of parallax. The sinusoidal voltage signal used to control the wave generator was also used to trigger a flash from a light-emitting diode placed in the field of view of the video camera. This flash (which occurred at precisely the same phase in each wave period) was used to calibrate the framing rate of the video camera against the driving period of the wave generator. Horizontal and vertical fiducial marks 10.0 cm apart on the window provided a scale for the recorded images.

The air-filled ball was subjected to waves 8.5 cm high at a frequency of 1.0 Hz. The motions of the ball were recorded for approximately 17 min, covering more than 1000 cycles of wave oscillation. The corn-oil-filled ball was subjected to waves with a height of 5.2 cm at a frequency of 1.5 Hz and was also filmed for approximately 17 min (1500 cycles).

A computer-controlled NEC PC-VCR was used to step through the SVHS video frame by frame. Each frame was digitized to 640×480 pixels at eight bits per pixel on a Perceptics Pixelpipe frame grabber. The images were stabilized using a computer-controlled Hotronics time-base corrector prior to digitization. The fiducial marks in the image allowed for the correction of any additional timing errors.

Graftek Imaging's Ultimage image-analysis package was used in conjunction with National Instruments LabView software to locate the table-tennis ball in the image. The image was binarized using a user-selected threshold, and the ball was then located using the Ultimage particle analysis subroutine. The centroid of the ball's image was calculated, giving the ball's location (*x* and *y* coordinates).

For comparison, our numerical model of *N. luetkeana* was modified to incorporate the dimensions and buoyancies of the physical models and the characteristics of the waves and water column in the wave tank. The locations of the ball predicted from our calculations could then be compared with those actually recorded.

Comparison between predictions and experiment were made on the basis of several characteristics. The power spectra of the *x*- and *y*-directed motions of the balls were used to describe how these motions are allocated among frequencies. Plots of *x versus y* (one manifestation of the phase space, in this case a phase plane) provide information about the repetitive nature of the ball's motion – regular, periodic motion of the ball yields a closed loop in the phase plane. In addition, the position (*x*,*y*) of the ball was noted at specific phases of the surface waves. A plot of values of *x versus y* for a single phase provides a Poincaré section of the ball's motion (for an explanation of Poincaré sections, see Moon, 1992). If this motion is periodic, the Poincaré section typically consists of a small number of discrete points.

The motion of the corn-oil-filled ball in the wave tank appeared to be chaotic and, for an additional comparison with the predictions of our numerical model, the largest Lyapunov exponent for each of the *x*- and *y*-axis motions was calculated using the program of Sprott and Rowlands (1992) based on the method of Wolf *et al.* (1985). The Lyapunov exponent is a measure of how rapidly two trajectories of the ball's motion move apart in phase space when these two points were initially very close together. A positive largest Lyapunov exponent can be indicative of chaos. See Moon (1992) for a more thorough introduction to the Lyanpunov exponent.

Numerical experiments

Seven aspects of the forces imposed on *N. luetkeana* were examined using our numerical model.

Effects of plant size

The model was used to calculate the maximum tension imposed on plants of lengths varying between 0.3 and 10.0 m. In these tests, the physical characteristics of the model plants (buoyancy, mass, stipe diameter and drag area) were set by the typical allometric relationships for *N. luetkeana* given in Table 3. The model plants were subjected to a series of 50 waves with a period of 10 s (typical of ocean swell on the west coast of North America) (Denny, 1995) and a fixed wave height. The water column depth was set at 10 m, a typical depth for *N. luetkeana*.

Effect of wave height

Hypothetical plants of a variety of stipe lengths were subjected to waves with τ=10 s and heights varying between 0.1 m and 7.8 m. This upper limit to wave height is governed by the tendency of waves to break if their heights exceed 0.78*d* (see Denny, 1988), and *d* was again 10 m. For each wave height, the plants were subjected to 50 waves. Plants with both allometric and isometric growth patterns (see below) were tested.

Effects of wave period

The effects of varying the wave period were explored by exposing plants of fixed length (2, 6 and 10 m) to waves of a fixed height (4 m) in water 10 m deep. Wave period was varied between 4 and 20 s, spanning the periods typical of oceanic seas and swell. Again, plants were exposed to 50 waves at each period and the maximum tension was noted for each wave cycle.

In each of these experiments, the maximum tension for each cycle of the surface waves was divided by the minimal cross-sectional area of the stipe to provide a measure of the maximum nominal stress placed on the stipe material. In addition, the vertical location of the point element, y_{mt}, was noted at the time of the maximum tension. This allows us to compare the maximum recorded stress (σ_{act}, a consequence, at least in part, of the motion of the alga) with the drag-induced stress σ_{stat} that a stationary plant would experience if its blade area were subjected to a unidirectional current with the maximum velocity that occurs at y_{mt}. This stress ratio,

$$R = \sigma_{act}/\sigma_{stat}\,, \tag{22}$$

Table 3. *The growth pattern in* Nereocystis luetkeana *and in the hypothetical plants used in the numerical experiments*

	Natural plants						Isometric 'small' plants		Isometric 'large' plants	
	α	β	*SEE*	*r*	*N*	*P*	α	β	α	β
Buoyancy (N)	0.328	1.657	0.010	0.961	25	<0.001	1.650	3	0.015	3
Mass (kg)	0.124	1.391	0.081	0.944	38	<0.001	0.860	3	0.003	3
Blade area (m^2)	0.140	1.270	0.083	0.913	49	<0.001	0.338	2	0.026	2
Minimum equivalent stipe radius (m)	0.00263	0.433	0.040	0.906	27	<0.001	0.00502	1	0.00071	1

The coefficients α and β refer to the equation: character of interest = αL^{β}, where *L* is stipe length.
SEE is the standard error of the regression estimate.

is an index of how the ability of the plant to move with the flow affects the stress its stipe encounters. A stress ratio of less than 1 indicates that going with the flow may be advantageous in terms of the tension imposed on the stipe.

Effect of blade proliferation at maturity

As noted above, when *N. luetkeana* plants have stipes long enough to reach the surface, the stipe stops increasing in length and the blades proliferate. To explore the mechanical consequences of this growth pattern, 'mature' plants were modeled by setting the stipe length equal to the water depth (10 m) and increasing the blade area by a factor of three above that predicted by the allometric growth equation of Table 3, a ratio commonly seen in the field. The overall plant mass was adjusted to account for the increase in frond size by noting that, in plants growing allometrically, approximately half the overall plant mass is due to the stipe. This mass was held constant and the remaining mass was multiplied by three.

Effects of plant shape

The consequences of allometric growth in *N. luetkeana* were explored by repeating the numerical experiment described above, but substituting hypothetical plants growing isometrically. These isometric plants had either the shape of a very small *N. luetkeana* (L=0.3 m) or of a large (natural) *N. luetkeana* with a stipe length equal to a typical water depth (L=10.0 m). The coefficients describing the pattern of growth in these isometric plants are given in Table 3. As with the allometric growth experiment, plants were subjected to 50 waves of fixed height and τ=10 s.

Effects of water depth

The effects of the depth of the water on the forces imposed on *N. luetkeana* were explored by exposing hypothetical allometric-growth plants of a fixed stipe length (2 m and a length equal to the water's depth) to waves of a fixed height (4 m) and period (10 s) at depths varying between 5 and 20 m. Plants were exposed to 50 waves at each depth and the maximum tension was noted in each wave cycle.

The estimates of stress made here can be placed in a biological context by comparing the calculated stress with the stress required to break the plant's stipe. Koehl and Wainwright (1977) measured the mean breaking strength of *N. luetkeana* in Washington state to be 3.64±2.20 MPa (mean ± S.D.). Johnson and Koehl (1994) report mean breaking stresses varying from 2.77±0.58 to 2.92±0.69 MPa (mean ± S.D.) for plants exposed to substantial water motion, again in Washington state. For the purpose of estimating the fraction of stipes broken by a given imposed stress, we assume that breaking strengths are normally distributed. Thus, a stress equal to the mean stress will break 50 % of stipes, a stress 1 standard deviation below the mean will break approximately 16 % of stipes, and a stress 2 standard deviations below the mean will break approximately 2 % of stipes (Zar, 1974).

Results

Morphology

The allometric relationships between stipe length and buoyancy, overall plant mass, frond area and minimal equivalent stipe radius are given in Table 3. In each case, the exponent β is significantly less than that expected for isometry, indicating that, as they grow towards the surface, these plants generally become more slender and relatively less buoyant. For example, overall plant mass, which would increase as L^3 for an isometrically growing plant, increases as only $L^{1.391}$. Buoyancy, which would similarly increase as L^3 in an isometrically growing plant, increases as $L^{1.657}$. Stipe diameter increases as $L^{0.433}$ rather than as L^1 as expected for isometry. This last relationship is in contrast to the results of Johnson and Koehl (1994), who found no correlation between stipe length and stipe diameter in their study in Washington state. Johnson and Koehl (1994) examined only mature *N. luetkeana*, however, and the restricted range of sizes used in their study may have obscured any relationship between stipe length and diameter. The different results found in the present study therefore do not necessarily mean that *N. luetkeana* has a different pattern of growth in California from that in Washington state.

Field tests

The tensions measured in the field closely match those predicted by our numerical model. The overall distribution of tensions are shown in Fig. 4. To create these graphs, the measured tensions were sampled every 0.5 s and the predicted tensions were sampled as close to every 0.5 s as allowed by the variable time step of the numerical integrator. The mean measured tension was 9.99±3.20 N (mean ± S.D., N=3112). The mean predicted tension was 9.48±2.77 N (N=2995). Thus, our numerical model predicts the mean tension within approximately 0.5 N, 5.1 % of the mean measured tension. Note that, for both the actual plant and the model, the mean tension is less than the plant's net buoyancy (12.51 N).

The mean maximum tension measured for the 119 waves examined in the field trial was 13.48±3.04 N (mean ± S.D.). The mean predicted maximum tension is 12.69±2.70 N. Our numerical model underestimates the mean maximum tension by an average of 0.79 N, only 5.9 % of the measured mean maximum tension. The mean fractional error of the predicted maximum tensions is 5.7 %.

A representative time series of measured and predicted tensions is shown in Fig. 5. In general, the predictions of the model closely follow the measured tensions, although there are occasions (as seen in the last third of this figure) when the phase of a predicted peak is shifted substantially from that measured and, on rare occasions, the numerical model misses entirely a peak in the measured tension. These deviations are probably due to the finite size of real plants (as opposed to the point element used in the model). If some fraction of the blades is moving in one direction while the rest of the plant moves in another, the resulting force could differ substantially (both in

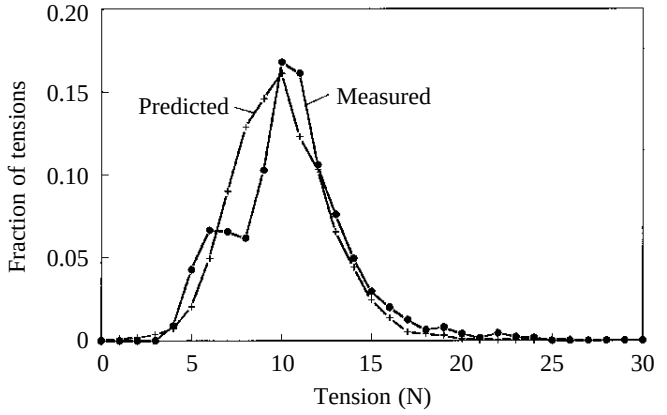

Fig. 4. A comparison of the distribution of stipe tensions recorded in the field (●) with those predicted by the numerical model (+). The mean measured tension is slightly higher than the mean predicted tension (see text).

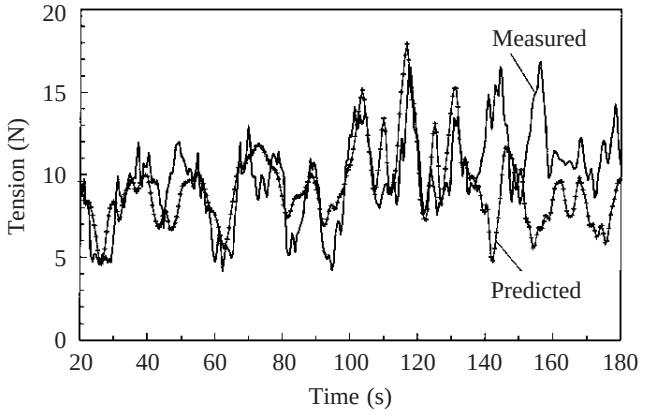

Fig. 5. A comparison of the time series of stipe tension measured in the field (thick, solid line) with the time series predicted by the numerical model (thin line with crossed data point).

magnitude and time) from the predicted force. Overall, the temporal shift between predicted and measured peak tensions is small. The mean difference in the time of peak tension is 0.56±2.28 s (mean ± S.D., N=119).

Laboratory experiments

The highly buoyant, air-filled ball behaved much like a pendulum (albeit in an inverted orientation because of the model's positive buoyancy), with a periodic motion under the influence of the surface waves (the spectrum for *y*-directed motion is shown in Fig. 6A). The spectra of the air-filled ball predicted by our numerical model closely match those measured in the wave tank (Fig. 6B).

The motions of the corn-oil-filled ball in the wave tank were much more complex (Fig. 7A). The reduction in buoyancy in this ball was sufficient to allow drag to propel the ball a substantial distance down into the water column, removing the tension on the tether. The ball then floated back towards the water's surface, again imposing a tension in its 'stipe'. The

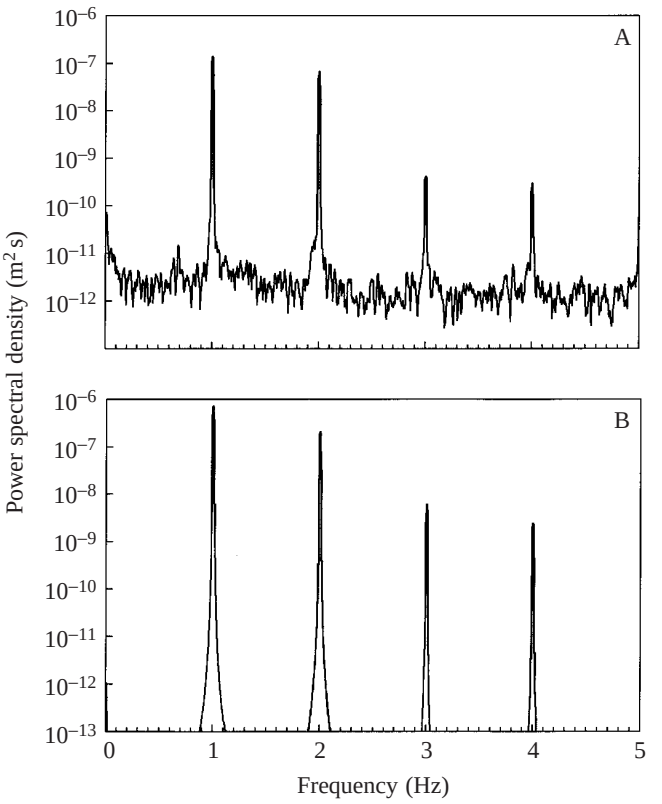

Fig. 6. The power spectra of (A) *y*-directed motion recorded in the wave tank for the air-filled ball and (B) *y*-directed motion predicted by the numerical model. The spectra from *x*-directed motion in the physical and numerical models show a similar match.

precise timing of this reimposition of tension relative to the phase of the wave-induced water motion had a drastic effect on the subsequent motion of the ball. Small shifts in the timing resulted in large changes in the ball's path.

The chaotic motion of the ball can be seen clearly in a Poincaré section (Fig. 7B), in which the horizontal location of the ball is plotted against its vertical location at one arbitrary phase of the driving frequency. The chaotic motion of the corn-oil-filled ball does not repeat itself, and its Poincaré plot tends to fill a certain range in the phase plane.

The sensitive coupling between the periodic motion of the water and the discontinuous tension on the tether is reflected in the power spectra recorded for the corn-oil-filled ball in the wave tank (the spectrum for *y*-directed motion is shown in Fig. 8A). A discrete peak is present at the driving frequency (1.501 Hz), but much of the energy of the ball's motion is spread across a range of lower frequencies. Broad peaks at 0.520 and 0.989 Hz in the *y*-spectrum are not integral subharmonics of the driving frequency. The chaotic motions of the corn-oil-filled ball are predicted by our numerical model. The power spectra are characterized by a spread of energy across frequencies below the driving frequency, and the magnitude of these spectral estimates is quite similar to those recorded in the wave tank (the spectrum for *y*-directed motion is shown in Fig. 8B).

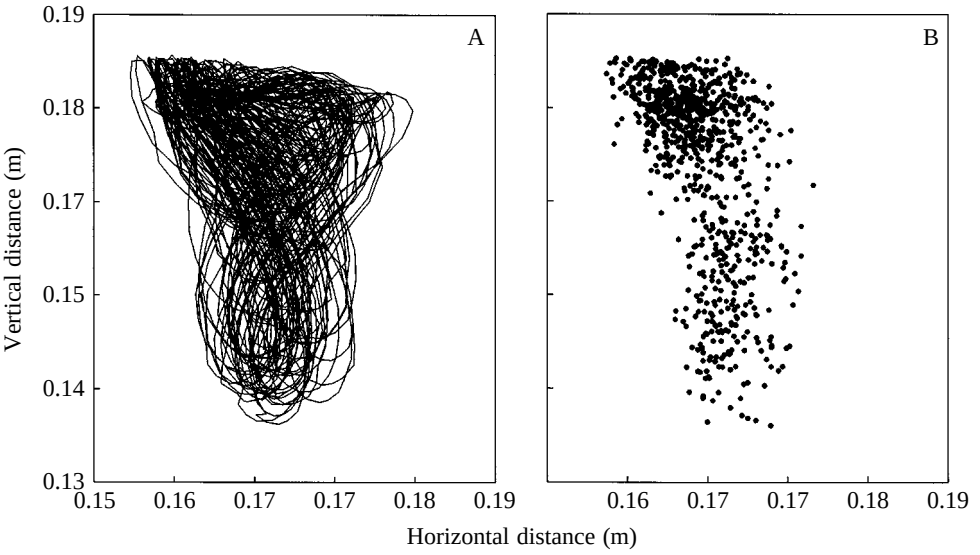

Fig. 7. The motion of the corn-oil-filled ball in the wave tank. (A) 300 wave cycles of motion. The ball does not follow the same track in each cycle. (B) A Poincaré section of the ball's motion taken at an arbitrary phase in the wave cycle. The broad spread of points is indicative of chaotic motion.

The largest Lyapunov exponent for the measured motion of the corn-oil-filled ball is positive: 0.317±0.055 (95 % confidence limits) for *x*-directed motion and 0.158±0.052 for *y*-directed motion, indicative of chaos. The largest Lyapunov number calculated for data from our numerical predictions is also positive: 0.304±0.038 (95 % confidence limits) for *x*-directed motion and 0.297±0.038 for *y*-directed motion, indicating that the numerical model (like the physical model) displays chaotic dynamics.

In summary, the predictions of our numerical model (spectra of *x*- and *y*-directed motions, Lyapunov exponents) closely match the measurements made in the wave tank, even for two quite dissimilar types of motion.

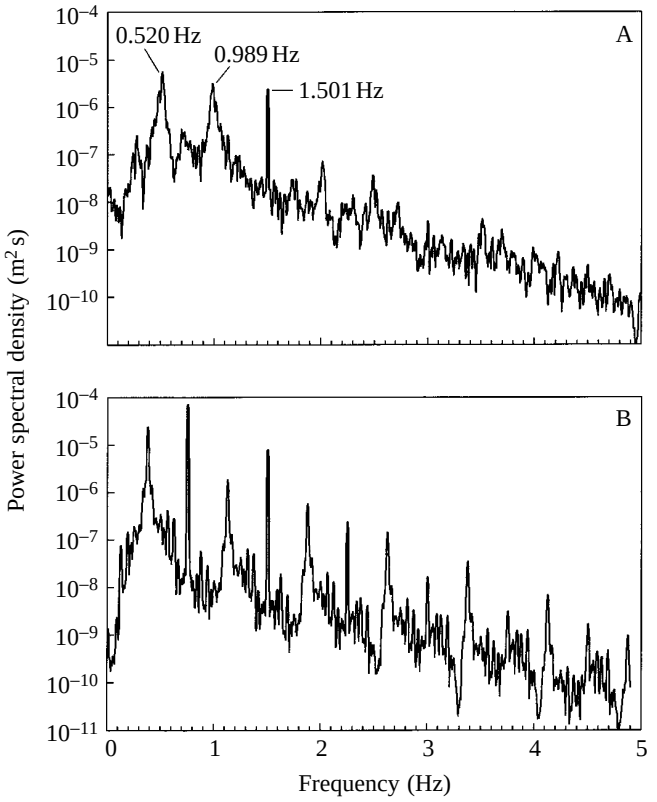

Fig. 8. The power spectra of *y*-directed motion of the corn-oil-filled ball in the wave tank (A) and in the numerical model (B). In each, there is a discrete peak at the driving frequency (1.50 Hz), but much of the variance in the ball's motion occurs at lower frequencies.

Predicted forces on N. luetkeana*: allometric growth*

Plant length

The allometric increase in minimal stipe diameter as a function of stipe length results in predicted dynamic stresses (tension per unit cross-sectional area) that are generally high for plants with stipes approximately 2 m long and low for stipes approximately 5–6 m long (Fig. 9A). The reduction in stress for stipes 5–6 m long is such that the stress these plants experience for waves 6 m high is no greater than that experienced under waves 4 m high. Above a length of 6 m, stress increases until the point element reaches the surface.

At the most stressful stipe length (2 m), a wave with a height equal to the breaking limit (7.8 m given a depth of 10 m) will impose a stress of approximately 1.5 MPa, 0.97–2.19 standard deviations below the mean breaking stress, depending on which estimate of strength is used (Koehl and Wainwright, 1977; Johnson and Koehl, 1994, respectively). Given the assumption of normally distributed breaking stresses, this suggests that 1.4–16.6 % of stipes 2 m long can be broken by extreme storm waves.

The static stress that would be applied to the plant by unidirectional flow is often less than that predicted by the model, with the result that the stress ratio, *R*, is generally greater than 1 (Fig. 9B). *R* is highest in short plants and generally decreases as plants grow longer. For wave heights of 4 m and greater, *R* may reach values in excess of 3.5 for stipe lengths of 1–2 m, indicating that in these short plants going with the flow increases (rather than decreases) the force imposed on the organism.

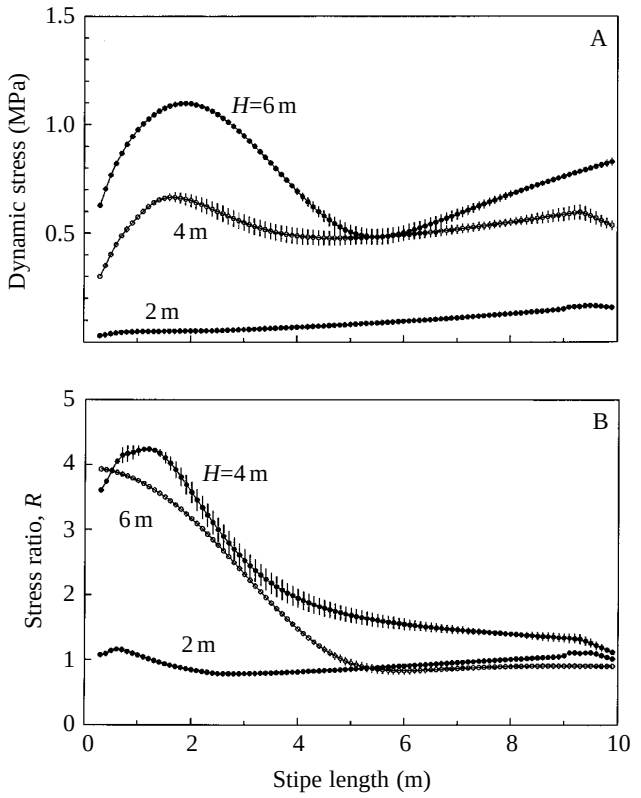

Fig. 9. The maximum stress (A) and maximum stress ratio (B) predicted for *N. luetkeana* as a function of stipe length. Each point is the mean of values recorded in 50 wave cycles and the error bars are standard deviations, an index of the variation in each value. *H*, wave height.

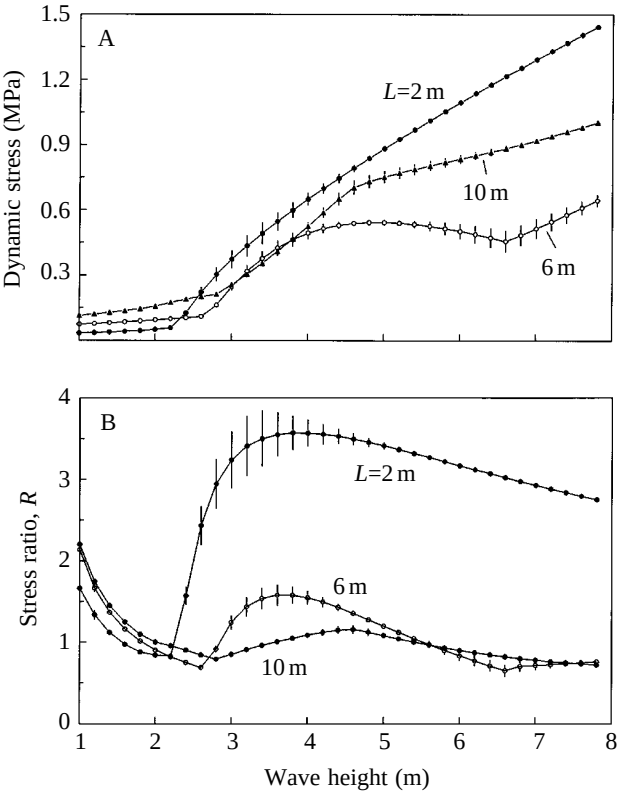

Fig. 10. The maximum stress (A) and maximum stress ratio (B) for *N. luetkeana* as a function of wave height. Each point is the mean of values recorded in 50 wave cycles and the error bars are standard deviations, an index of the variation in each value. *L*, stipe length.

Wave height

Predicted maximum dynamic stresses and stress ratios are shown as a function of wave height in Fig. 10 for plants of selected stipe lengths (2, 6 and 10 m) growing allometrically in water with d=10 m. Maximum dynamic stress generally increases with increasing wave height (Fig. 10A), although in plants 6 m long stress remains relatively constant above a wave height of 4 m.

The ratio of dynamic to static forces varies considerably with wave height (Fig. 10B), but is generally largest in small plants, such as the 2 m plant used in this example. In this case, R peaks at a value of 3.6 for a wave height of 3.8 m, an indication that much of the load on these plants is due to dynamic forces. For plants 10 m long, R is generally low, varying only slightly above and below a value of 1.

Wave period

The effects of wave period depend on stipe length (Fig. 11). For a short allometric-growth plant (L=2 m), stress is maximal when waves have a period of 10 s (Fig. 11A). In contrast, when the plant is as long as the water is deep (10 m), stress is maximal when the wave period is approximately 5.5 s. The corresponding stress ratios (Fig. 11B) generally decrease with increasing wave period.

Predicted consequences of blade proliferation at maturity

Wave height

Increasing blade area and mass by a factor of 3 in a plant 10 m long increases the predicted stress imposed on the stipe at all wave heights, but by a factor that is generally less than 3 (Fig. 12A). These 'mature' plants apparently benefit from going with the flow: the stress ratio is uniformly less than 1 (Fig. 12B), and for wave heights in excess of 4 m can be as low as 0.55, indicating that these plants experience only 55 % of the force they would feel if their blades were subjected to unidirectional flow.

The maximum stress imposed on a mature plant by waves with a height equal to the breaking limit (for d=10 m) is approximately 2 MPa, 0.75–1.33 standard deviations below the measured means of breaking stress. Given the assumption of normally distributed breaking stresses, this suggests that 9.1–22.8 % of mature plants could be broken by extreme storm waves.

Wave period

The stress and stress ratio occurring in mature *N. luetkeana* plants is maximal at short wave periods (<8 s), the precise location of the maximum depending on wave height (Fig. 13A,B). At long wave periods (>16 s), the stress ratio

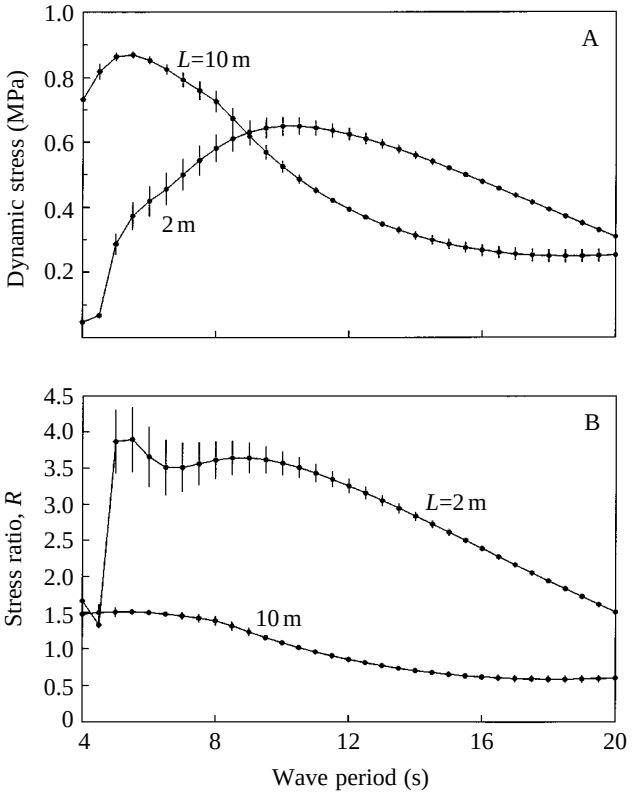

Fig. 11. The maximum stress (A) and maximum stress ratio (B) for *N. luetkeana* as a function of wave period. Each point is the mean of values recorded in 50 wave cycles and the error bars are standard deviations, an index of the variation in each value. *L*, stipe length.

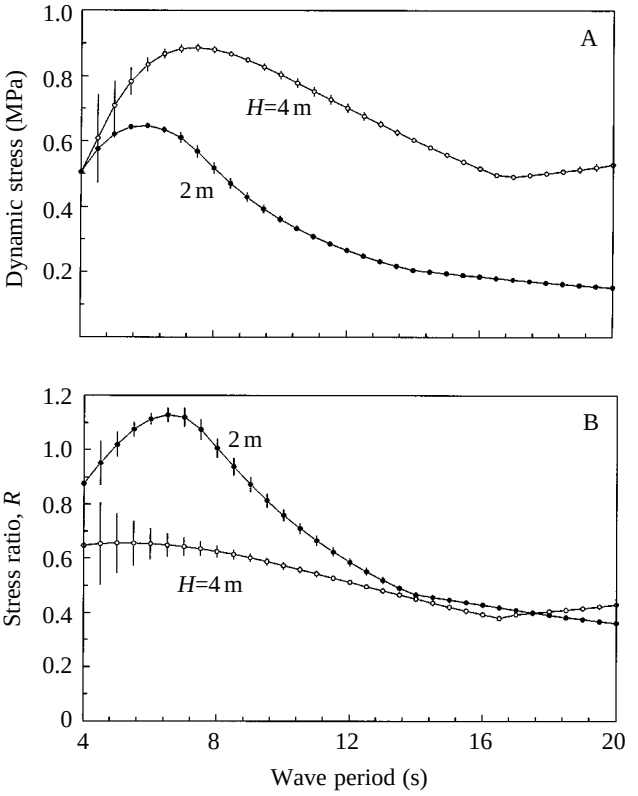

Fig. 13. The maximum stress (A) and maximum stress ratio (B) for mature *N. luetkeana* (stipe length *L*=10 m, with a threefold proliferation of blade area) as a function of wave period. Each point is the mean of values recorded in 50 wave cycles and the error bars are standard deviations, an index of the variation in each value. Depth 10 m. *H*, wave height.

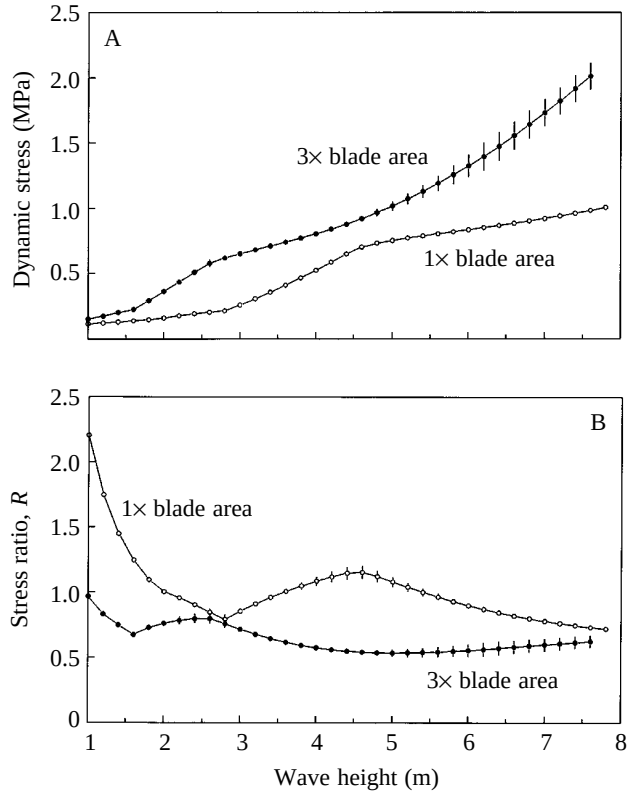

Fig. 12. The maximum stress (A) and maximum stress ratio (B) for mature *N. luetkeana* (stipe length *L*=10 m, with a threefold proliferation of blade area) as a function of wave height. Each point is the mean of values recorded in 50 wave cycles and the error bars are standard deviations, an index of the variation in each value. Note that the stress ratio of the mature plants is uniformly less than 1, indicating that these plants receive a benefit from 'going with the flow'. The curve for a 10 m long plant prior to blade proliferation is shown for reference. Depth 10 m, period 10 s.

may be less than 0.4, indicating that going with the flow is exceptionally advantageous under these conditions (Fig. 13B).

Predicted consequences of isometric growth: 'large' shape

Plant length

The pattern of forces imposed on a plant that grows with the shape of a normal *N. luetkeana* 10 m long are similar to those seen in plants growing allometrically. The peaks in stress and stress ratio seen in short allometric-growth plants occur in these isometric-growth plants, but at slightly lower values. For example, when waves are 6 m high, the peak stress in the isometric 'large'-shape plant is 0.88 MPa compared with 1.10 MPa in the allometric plant. For stipe lengths in excess of

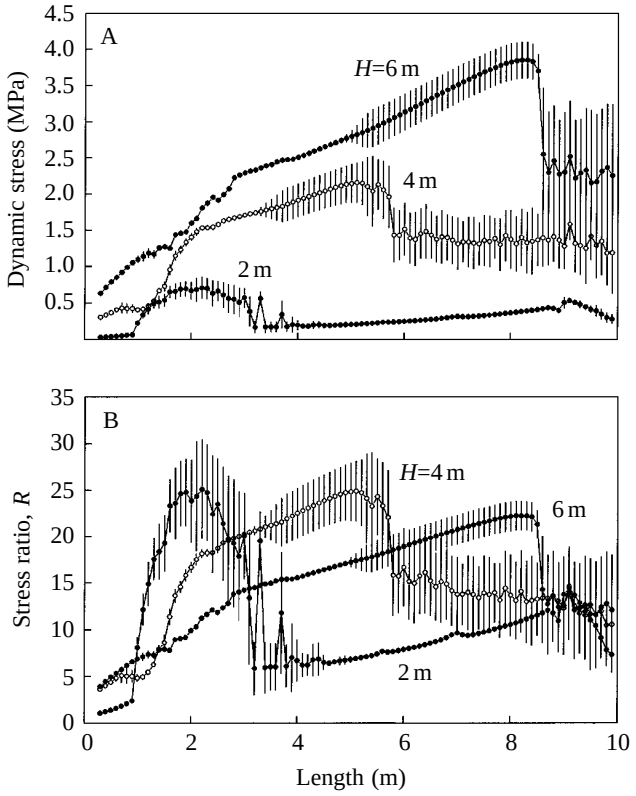

Fig. 14. The maximum stress (A) and maximum stress ratio (B) as a function of stipe length for hypothetical plants growing with the shape of a small (0.3 m long) *N. luetkeana*. Each point is the mean of values recorded in 50 wave cycles and the error bars are standard deviations, an index of the variation in each value. *H*, wave height.

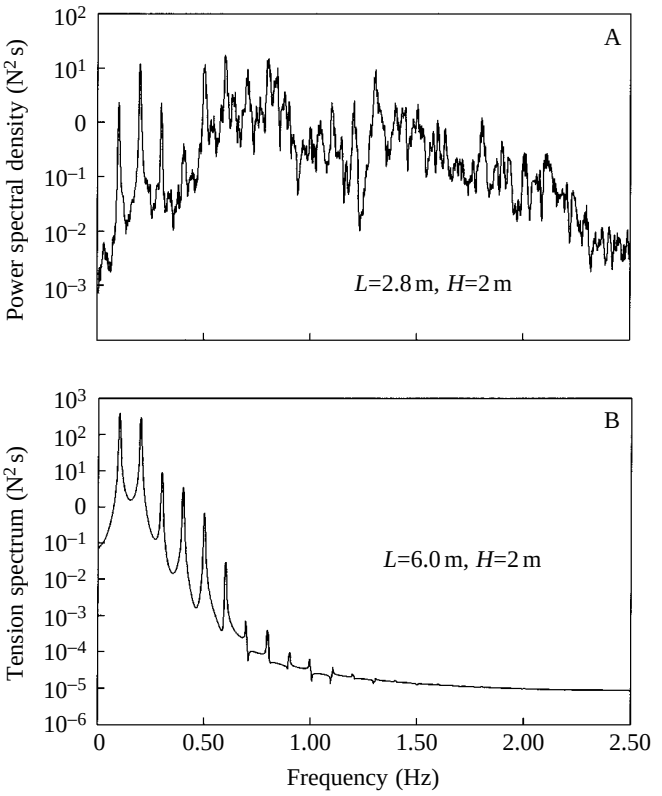

Fig. 15. (A) The power spectrum of tensions predicted by the numerical model for a hypothetical plants with a 'small' shape (L=2.8 m, H=2 m, τ=10 s, d=10 m). The chaotic dynamics of the plant are evident in the noisy spectrum. (B) The power spectrum for a 'small'-shaped hypothetical plant under the same conditions as for A, but with L=6 m. The discrete peaks in B are indicative of periodic motion. *L*, stipe length; *H*, wave height; τ, wave period; *d*, water column depth.

3 m, the isometric 'large'-shape plants behave in a similar manner to allometrically growing plants, as expected.

Wave height and period

The variation in stress and stress ratio as a function of wave height and period are similar between isometric-growth 'large'-shape plants and allometric-growth plants. The sole notable difference is that the tension and stress ratio in 'large'-shape plants with short stipes is slightly less than that in the corresponding allometric plants.

Predicted consequences of isometric growth: 'small' shape

Plant size

Plants growing isometrically with the shape of a 0.3 m long allometric-growth plant have a complicated behavior (Fig. 14). In general, the stress and stress ratio in these plants are higher than those in plants that grow allometrically (Fig. 9). However, the mean stress at a given wave height can vary drastically with a small change in stipe length. Consider, for example, the variation in stress and stress ratio for plants exposed to waves 2 m high. For stipe lengths between 1.0 and 5.0 m, stresses and stress ratios are much increased above the smooth trend found at other stipe lengths. Furthermore, in this range of anomalous stress, the maximum calculated stresses vary substantially between successive waves. For certain lengths in this range (e.g. 2.10 m), the pattern of variation in maximum force eventually settles down to a periodic repetition, alternating between two different tensions on consecutive waves. For other lengths (e.g. 1.2 m), maximum forces repeat every four waves. At still other lengths (e.g. 2.8 m), the motion of the isometric plant appears to be chaotic. For example, the power spectra of *x*- and *y*-directed motion and stipe tension in a 2.8 m long plant subjected to waves 2 m high exhibit some of the broad-band noise typical of deterministic chaos. This is particularly evident for the power spectrum of tension (Fig. 15A). The noise in this spectrum is best judged by comparison with the spectrum obtained for a longer isometric-growth plant subjected to the same flow regime (Fig. 15B). The spectrum for this longer plant exhibits the discrete peaks characteristic of a complicated but strictly periodic motion. A Poincaré section of the motion for the 2.8 m long isometric plant is shown in Fig. 16. The 1000 points in this figure tend to fill a region of phase space and exhibit none of the regularity expected of periodic or quasiperiodic motion.

When plants with an isometric 'small' shape are subjected

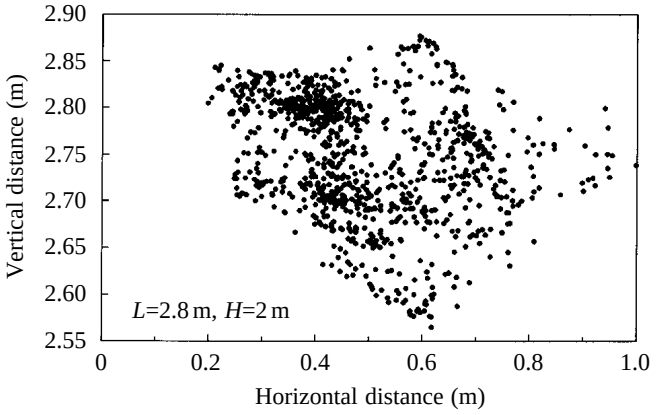

Fig. 16. A Poincaré section of the motion of a 'small'-shaped hypothetical plant (H=2 m, τ=10 s, d=10 m) at an arbitrary phase in the wave cycle. The broad spread of points is indicative of chaos. L, stipe length; H, wave height; τ, wave period; d, water column depth.

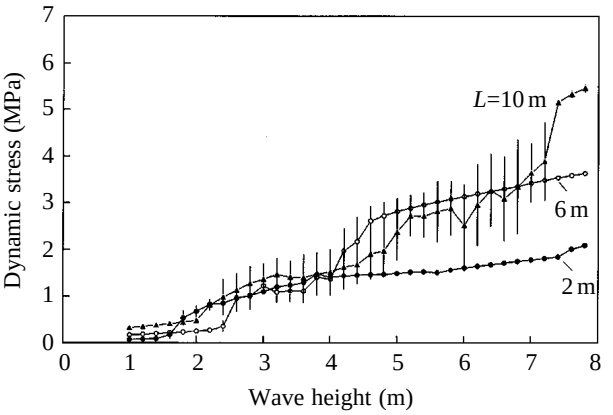

Fig. 17. Maximum dynamic stress as a function of wave height for hypothetical plants growing with the shape of a small *N. luetkeana*. Each point is the mean of values recorded in 50 wave cycles and the error bars are standard deviations, an index of the variation in each value. L, stipe length.

to waves higher than 2 m, a similar 'bump' in stress is seen for a range of stipe lengths (Fig. 14A,B), and a shift from periodic to chaotic motion is also observed. The 'bump' in stress extends over a much larger range of lengths, however, and the shift from periodic to chaotic motion occurs at longer stipe lengths. In this case, the shift to chaotic motion may be accompanied by a decrease (rather than an increase) in mean maximum tension and stress. For example, when waves are 4 m high, plants with stipes longer than approximately 5.5 m exhibit maximum tensions that vary drastically from one wave to the next, but the mean maximum tension is substantially lower than that at slightly shorter stipe lengths (Fig. 14A). As with the example discussed above, the maximum tension may alternate between two values on successive waves, may return to the same value every four waves or may be aperiodic (that is, chaotic). Note that the shift to variable maximum stresses for waves 4 m high occurs at stipe lengths too short to allow the point element to encounter the surface. When the waves are 6 m high, the shift to variable maximum tensions does not occur until plants are approximately 8.5 m long (Fig. 14), at which point they may intersect the surface in wave troughs. In this case, the possibility that the variation in maximum tension is driven by surface effects cannot be ruled out.

We conclude from these data that plants growing isometrically with a 'small' shape are (for certain ranges of stipe length and wave height) subjected to dynamic stresses that are highly variable and on average drastically different from those acting on plants of the same shape but with longer or shorter stipes and are also different from those imposed on plants growing allometrically. In some cases, these anomalous stresses are much larger than those imposed on plants growing allometrically. For certain stipe lengths and wave heights, these anomalous tensions arise in association with chaotic motions of the plant.

Wave height

The complexity of motion in isometric-growth 'small'-shape plants is further exhibited when stress is examined as a function of wave height (Fig. 17). Average maximum stress generally increases with increasing wave height regardless of the length of the plant's stipe, but the trend is noisy, with the overall maximum stress being found in plants of different lengths at different wave heights. Stress ratios (data not shown) vary among wave heights with no clear pattern, although they are uniformly much in excess of 1 (15.6±4.7, mean ± S.D.) and reach values as high as 25.

Wave period

The stresses occurring in isometric-growth 'small'-shape plants with a stipe 2 m long are maximal for wave periods between 6 and 10 s (Fig. 18). At longer periods, this parameter decreases dramatically. The behavior of isometric 'small'-shape plants with a stipe length of 10 m is highly erratic. Any underlying pattern in stress as a function of wave period is

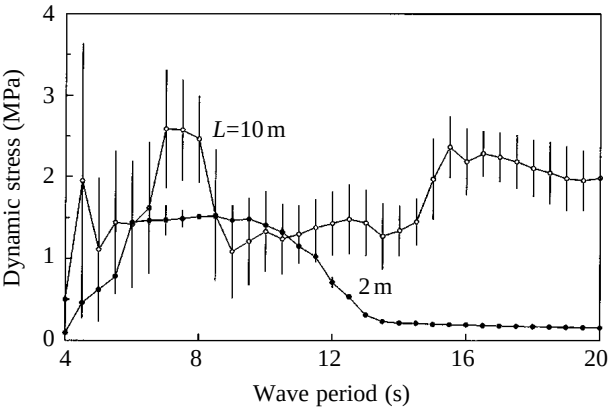

Fig. 18. Maximum stress as a function of wave period for hypothetical plants growing with the shape of a small *N. luetkeana*. Each point is the mean of values recorded in 50 wave cycles and the error bars are standard deviations, an index of the variation in each value. L, stipe length.

obscured by the chaotic motions of the plant. The average stress ratio is 13.6±7.9 (mean ± S.D.). Note that, at a period of 7–8 s, plants 10 m long subjected to waves 4 m, as used in this experiment, experience stresses that on average approach the mean breaking stress of *N. luetkeana* measured by Johnson and Koehl (1994) (2.77±2.92 MPa).

In summary, hypothetical individuals that grow isometrically with the shape of small *N. luetkeana* plants encounter stresses that are generally large relative to plants with allometric growth and can behave erratically when exposed to wave-induced flows. For certain combinations of wave height and stipe length, the stresses accompanying these erratic motions can be more than 10 times those found in allometric plants and, for long stipes, can be large enough to break a substantial fraction of stipes.

Predicted effects of water depth: allometric-growth plants

The effects of water depth are sensitive to the length of the plant. For allometric plants with a stipe length of 2 m, the tension and stress in the stipe decrease monotonically as water depth increases (Fig. 19). In contrast, the tension and stress in a plant whose stipe is as long as the water is deep vary in a more complex fashion. For example, stress reaches a maximum at a depth of 8 m and has a local minimum at a depth of 15 m.

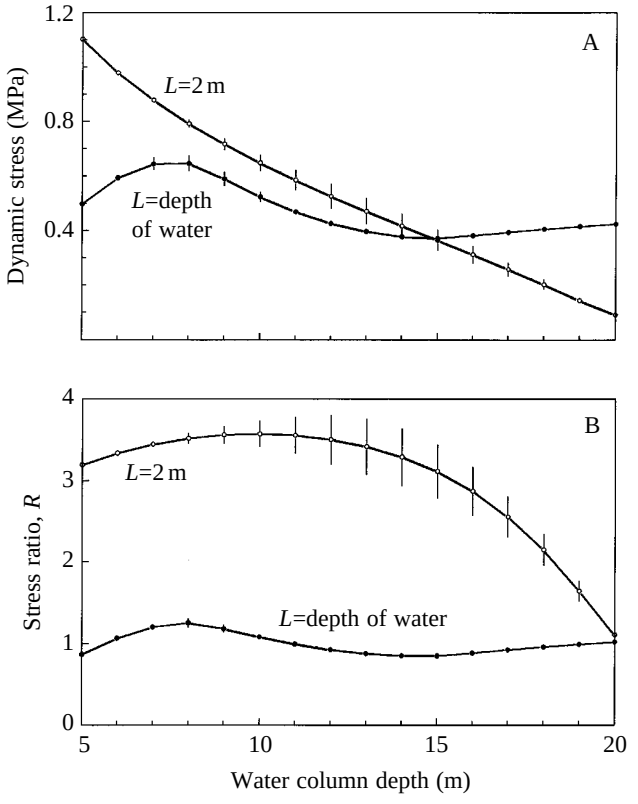

Fig. 19. The maximum dynamic stress (A) and maximum stress ratio (B) for allometric *N. luetkeana* as a function of the depth of the water column. Each point is the mean of values recorded in 50 wave cycles and the error bars are standard deviations, an index of the variation in each value. *L*, stipe length.

Discussion

In the present study, we propose a simple numerical model for the kinetics of *N. luetkeana* and have shown that these calculations accurately predict the motions of small-scale physical models and the stresses imposed on an actual *N. luetkeana* plant in the field. These preliminary tests give us tentative confidence that our numerical model is a reasonably accurate depiction of the kinetics of the bull kelp, and we have used the model to explore the roles that plant size and allometry, wave height and period and water depth play in the maximum forces imposed on this kelp's stipe. The result is a preliminary sketch of the highly complex motion of this flexible plant when exposed to wave-induced flows. Three primary conclusions can be drawn from this sketch.

Wave-induced forces alone can break only a small fraction of N. luetkeana *stipes*

The results presented in Fig. 12A show that even when waves are at their maximum height, they are capable of breaking only 9–23 % of the stipes of a population of mature kelps growing in water 10 m deep. This is consistent with the results reported for other large kelps. For example, Friedland and Denny (1995) found that intact stipes of the feather boa kelp *Egregia menziesii* were quite capable of resisting the water motion associated with waves in the surf zone, and Utter and Denny (1996) predicted that even extreme storm waves were capable of breaking only 12–17 % of stipes in the giant kelp, *M. pyrifera*.

Going with the flow is advantageous, but only for mature plants

The stress ratio of a 10 m long mature *N. luetkeana* is substantially less than 1 for all wave heights and periods (Fig. 12B), suggesting that these large individuals receive an advantage from their ability to move with the surrounding water. The advantage of going with the flow does not apply, however, to juvenile *N. luetkeana*. For example, plants 2 m long can experience stresses capable of breaking 1–16 % of stipes (Fig. 9A), and two-thirds of this stress can be attributed to dynamic loading (R=3, Fig. 9B). Thus, it appears that *N. luetkeana* must grow through a length range in which going with the flow is disadvantageous before finally reaching a size at which flexibility is beneficial.

Allometric growth has a strong effect on the forces encountered

Our numerical model suggests that if *N. luetkeana* were to grow isometrically, maintaining the shape it had as a juvenile plant, the forces encountered would be increased (Fig. 17) to the extent that storm waves (wave heights 5–6 m) would impose stresses in excess of the mean breaking stress. Much of this increase in force would be due to dynamic loading – the mean stress ratio in these 'small'-shape plants is predicted to exceed 10 for most wave heights and stipe lengths, and can be as high as 25 (Fig. 14B). Thus, if *N. luetkeana* were to grow

isometrically, going with the flow would be highly disadvantageous.

The increase in stress in 'small'-shape isometric-growth plants is due to two factors. First, small plants have a relatively large blade area and mass for their length, which would directly increase their drag and potentially increase their inertial load. 'Small' shape could thereby increase the mean maximum force exerted on the stipe. Second, for certain combinations of wave height, wave period and plant length, isometric-growth 'small'-shape plants are predicted to experience a maximum force that varies from one wave to the next, even when wave height and period are constant. The largest of these variable forces can greatly exceed the mean. As a result, the dynamics associated with the juvenile shape can substantially increase the risk of breakage in the stipe.

In summary, the results reported here suggest that going with the flow cannot be a mechanical panacea in wave-swept algae. Unless a plant's shape is adjusted appropriately during growth and the plant grows to sufficient size (a length approaching the water's depth), the disadvantages of inertial loading outweigh the advantages of reduced relative velocity. Note that other kelps, such as *Laminaria saccharina*, have been shown to be capable of adjusting their shape in direct response to imposed forces (Gerard, 1987), suggesting the possibility that the observed allometric growth in *N. luetkeana* could itself be a response at least in part to the dynamic forces imposed on the plant.

The role of chance

For a plant whose dynamics are chaotic (e.g. a bull kelp growing isometrically with a 'small' shape), the intrinsic variability in the plant's dynamics injects an element of chance into the forces imposed on the organism. If by chance a plant's blade mass comes to the end of its tether at just the right instant in the wave's phase, can the resulting force increase without limit? If this were true, plants might be broken even when the wave height was constant and relatively small. This scenario, coupled with the fact that we do not observe chaotic motion in *N. luetkeana* plants with a 'natural' shape, could be used in an evolutionary explanation of why the bull kelp grows with the form that it does.

This argument is only partially supported, however, by an examination of the probability distribution of forces imposed on chaotic kelps. We have used our model to expose a 'small'-shape plant 2.8 m long to monochromatic waves 2 m high (d=10 m, τ=10 s), a flow regime that we have shown induces chaotic dynamics. The plant was exposed to 1500 waves and the maximum stress was recorded for each wave cycle. A representative segment of this record is shown in Fig. 20. Maximum stress does indeed vary erratically from one cycle to the next, but there appear to be limits to this variation. The height of all the higher peaks is approximately the same, as is the depth of the lower valleys. This impression is borne out when the cumulative probability curve is calculated (Fig. 21). There is no evidence of a tail of rare large forces in this curve, suggesting that there may be a stringent limit to the maximum

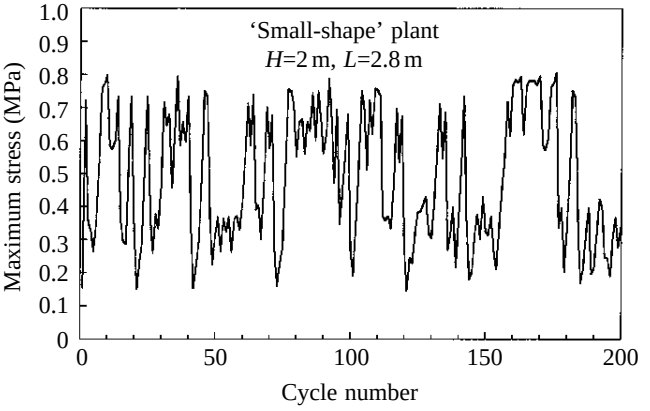

Fig. 20. A time series of the maximum stresses recorded in each of 200 wave cycles for a 'small'-shaped hypothetical plant undergoing chaotic motion. *L*, stipe length; *H*, wave height.

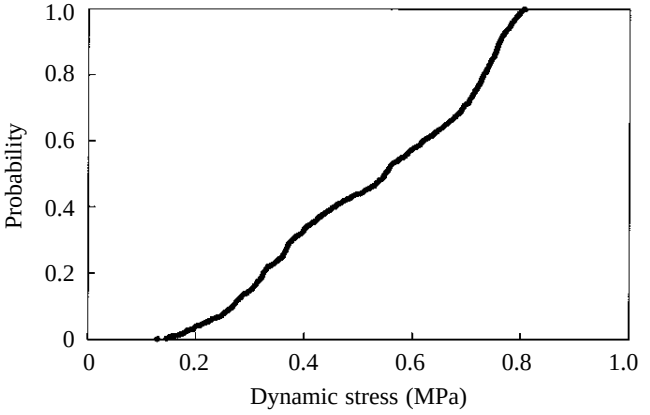

Fig. 21. The cumulative probability distribution of maximum stresses from 1500 wave cycles for a 'small'-shaped hypothetical plant undergoing chaotic motion.

force that will occur due to chaotic motion. If this is indeed so, it implies that chaotic dynamics, while capable of increasing the stress imposed on a plant, does so only within limits. In this case (H_s=2 m), the limit is approximately 0.8 MPa, a stress that would break only a tiny fraction of stipes. Therefore, if the upper limit to the stress imposed by chaotic motion is less than the strength of the plant's stipe material, the presence of chaos does not necessarily imply a reduction in survivorship.

Caveats

The simple numerical model proposed here is only a first step towards a complete understanding of the dynamics of giant kelps. For example, we have drastically simplified the plant's dynamics by assuming that mass and area are present at a single point whereas, in an actual plant, mass and area are distributed both along the stipe and across the blades. As noted previously, this oversimplification on our part may help to explain the occasional deviations of the model's predictions from the forces measured in the field (Fig. 5). It would be feasible (although computationally intensive) to construct a multi-element,

distributed-mass model to predict these more complicated motions. It may also be advantageous in future models to account for the forces associated with convective accelerations, the slight bending stiffness of *N. luetkeana* stipes and the nonlinear aspects of near-shore waves. In the meantime, we are encouraged that a model as simple as ours appears to explain much of the dynamic behavior of *N. luetkeana*.

Our numerical results suggest that, by being large enough, kelps can indeed benefit from going with the flow, and we concur with others (e.g. Koehl and Wainwright, 1977; Koehl, 1986) that this reduction in hydrodynamic forces may have played a role in the evolution of shape and material properties in these plants. There are, however, several alternative or additional factors that could select for large size in kelps. (1) Light is rapidly attenuated by coastal sea water, and any morphological shift that allows blades to come close to the surface thus has the potential to increase a plant's photosynthetic output. (2) A frond adjacent to a rocky substratum is liable to be tattered by contact with the rock and may be at an increased risk of herbivory. In this respect, it may be advantageous to move the fronds away from the substratum. This has been accomplished in many species by the evolution of a woody, cantilever-like stipe (see Gaylord and Denny, 1997), but the support of one or more buoyant floats (as seen in feather boa, bull and giant kelps) appears to be a viable alternative. (3) Lastly, for *N. luetkeana*, the ultimate size of the blades determines the size of the plant's sporophylls. Thus, increased size (if accompanied by reasonable survivorship) will increase reproductive output. It seems reasonable that any or all of these factors could have provided additional guidance in the evolution of large size in *N. luetkeana*.

If big is good, why, then, have more kelps not followed the same path? Large size is, after all, the exception rather than the rule in wave-swept plants. At least part of the answer may lie in the large stresses placed on relatively small plants, as seen here for 2 m long *N. luetkeana*. If evolving plants just grew longer without any adjustment to their shape, our model suggests that dynamic forces imposed by waves could form a barrier to further growth. Only after an appropriate allometry had been achieved could plants grow through this hydrodynamically enforced bottleneck in the presence of substantial wave action.

It should be noted, however, that wave heights vary seasonally in a predictable fashion, and intervals of calm can occur even in the stormiest of seasons. Thus, it is possible for plants to avoid the consequences of disadvantageous size or shape by growing through the bottleneck at a time when large waves are absent. *N. luetkeana* may well take advantage of this opportunity to hedge its bets. Plants begin to grow in the early spring, when wave heights are generally lower than those during the winter storm season. Furthermore, *N. luetkeana* is among the fastest growing plants on earth; its stipe length increases by an average of 10 cm per day (Abbott and Hollenberg, 1976) and at times can increase by as much as 25 cm per day (Duncan and Foreman, 1980). Given this rate of stipe extension, only a few days would be required to grow through the range of stipe lengths for which dynamic loading is severe. If these few days could be synchronized with periods of small waves, *N. luetkeana* could avoid altogether the consequences of dynamic loading at small size.

Finally, we note two other factors that could affect the predictions of the probability of stipe breakage made here. First, Koehl and Wainwright (1977) found that the majority of bull kelp stipes broken at their field sites in Washington state were either tangled with other stipes or had been weakened by herbivory. If tangling is present, the predictions made here are likely to underestimate the rates at which stipes are broken in natural populations. In this respect, the ultimate fate of a plant may be governed not only by its mechanical design (the properties of its materials and its shape) but also by its interactions with predators and neighbors. Second, large waves are most likely to occur in the winter, when the blade mass of *N. leutkeana* is typically small. Thus, the predictions made here regarding stipe breakage could be overestimates, in that they assume that waves of maximal height can act on plants with their full blade mass.

A final note on chaos in kelps

In the results reported here, we have only begun to explore the nature and consequences of chaotic dynamics in the simple point-element/tether system of our numerical model. What is the route to chaos for this system? Our preliminary results suggest that period doubling (see Moon, 1992) may be the answer, based on our observation of periodicity in the maximum force of both two and four times the forcing period. We have not, however, examined the matter in detail. Precisely where are the boundaries between periodic and chaotic motion? What particular aspects of plant size and shape govern the transition to chaos? We simply do not know. We hope that by reporting our preliminary findings here, others will be stimulated to pursue this intriguing mechanical system in greater depth. A first step in this direction has been taken by Gottlieb (1997), who examined the motion of an inverted, elastic pendulum exposed to wave-driven hydrodynamic motions. This model is similar to our kelp model, but does not include the discontinuity in the stiffess of the tether. Gottlieb found chaotic motions in his system similar to those reported here.

We thank B. Hale, J. Leichter, S. Wing, G. Villa, L. Roberson and T. Nicholson for their assistance with the field and laboratory work, O. Gottlieb for insight regarding chaos, and Drs S. Monismith and J. Koseff for the use of the wave tank in Stanford's Environmental Fluid Mechanics Laboratory. Freya Sommer lent her artistic talents to Fig. 1. Portions of this work were supported by NSF Grants OCE 9115688 and OCE 9313891 to M.W.D.

References

ABBOTT, I. A. AND HOLLENBERG, G. J. (1976). *Marine Algae of California.* Stanford, CA: Stanford University Press.

BATCHELOR, G. K. (1967). *An Introduction to Fluid Dynamics.* Cambridge, UK: Cambridge University Press.

BEAUCHAMP, J. J. AND OLSON, J. S. (1973). Correction for bias in regression estimates after logarithmic transformation. *Ecology* **54**, 1403–1407.

BOLE, J. B. AND HSU, E. Y. (1969). Response of gravity waves to wind excitation. *J. Fluid Mech.* **35**, 657–675.

CARRINGTON, E. (1990). Drag and dislodgment of an intertidal macroalga: consequences of morphological variation in *Mastocarpus papillatus* Kützing. *J. exp. mar. Biol. Ecol.* **139**, 185–200.

DAHLQUIST, G. AND BJÖRCK, Å. (1974) *Numerical Methods*. Englewood Cliffs, NJ: Prentice-Hall.

DAYTON, P. K., CURRIE, V., GERRODETTE, T., KELLER, B. D., ROSENTHAL, R. AND VENTRESCA, D. (1984). Patch dynamics and stability of some California kelp communities. *Ecol. Monogr.* **54**, 253–289.

DENNY, M. W. (1988). *Biology and the Mechanics of the Wave-Swept Environment.* Princeton, NJ: Princeton University Press.

DENNY, M. W. (1995). Predicting physical disturbance: mechanistic approaches to the study of survivorship on wave-swept shores. *Ecol. Monogr.* **65**, 371–418.

DENNY, M. W., DANIEL, T. L. AND KOEHL, M. A. R. (1985). Mechanical limits to size in wave-swept organisms. *Ecol. Monogr.* **55**, 69–102.

DUNCAN, M. J. (1973). *In situ* studies of growth and pigmentation of the phaeophycean *Nereocystis luetkeana*. *Helgolander wiss. Meeresunter.* **24**, 510–525.

DUNCAN, M. J. AND FOREMAN, R. E. (1980). Phytochrome-mediated stipe elongation in the kelp *Nereocystis* (Phaeophyceae). *J. Phycol.* **16**, 138–142.

ECKART, C. (1952). The propagation of waves from deep to shallow water. In *Gravity Waves*. National Bureau of Standards, Circular no. **521**, 165–173.

FOSTER, M. S. AND SCHIEL, D. R. (1985). The ecology of giant kelp forests in California: A community profile. *U.S. Fish Wild. Serv. Biol. Rep.* **85**.

FRIEDLAND, M. T. AND DENNY, M. W. (1995). Surviving hydrodynamic forces in a wave-swept environment: consequences of morphology in the feather boa kelp *Egregia menziesii* (Turner). *J. exp. mar. Biol. Ecol.* **190**, 109–133.

GAYLORD, B., BLANCHETTE, C. A. AND DENNY, M. W. (1994). Mechanical consequences of size in wave-swept algae. *Ecol. Monogr.* **64**, 287–313.

GAYLORD, B. AND DENNY, M. W. (1997). Flow and flexibility. I. Effects of size, shape and stiffness in determining wave forces on the stipitate kelps *Eisenia arborea* and *Pterygophora californica*. *J. exp. Biol.* **200**, 3141–3164.

GERARD, V. A. (1987). Hydrodynamic streamlining of *Laminaria saccharina* Lamour in response to mechanical stress. *J. exp. mar. Biol. Ecol.* **107**, 237-244.

GOTTLIEB, O. (1997). Bifurcations of a nonlinear small-body ocean mooring system excited by finite amplitude waves. *ASME J. Offshore Mech. Arctic Eng.* (in press).

HSU, E. Y. (1965). A wind wave research facility. Stanford University Department of Civil Engineering Technical Report no. 57.

JOHNSON, A. S. AND KOEHL, M. A. R. (1994). Maintenance of dynamic strain similarity and environmental stress factor in different flow habitats: thallus allometry and materials properties of a giant kelp. *J. exp. Biol.* **195**, 381–410.

KINSMAN, B. (1965). *Wind Waves*. Englewood Cliffs, NJ: Prentice-Hall.

KOEHL, M. A. R. (1984). How do benthic organisms withstand moving water? *Am. Zool.* **24**, 57–70.

KOEHL, M. A. R. (1986). Seaweeds in moving water: form and mechanical function. In *On the Economy of Plant Form and Function* (ed. T. J. Givnish), pp. 603–634. Cambridge: Cambridge University Press.

KOEHL, M. A. R. AND WAINWRIGHT, S. A. (1977). Mechanical design of a giant kelp. *Limnol. Oceanogr.* **22**, 1067–1071.

LONGUET-HIGGINS, M. S. (1952). On the statistical distribution of the height of sea waves. *J. mar. Res.* **11**, 245–266.

MILOH, T. (1994). Pressure forces in deformable bodies in non-uniform inviscid flows. *Q. J. Mech. appl. Math.* **47**, 635–661.

MOON, F. C. (1992). *Chaotic and Fractal Dynamics*. New York: John Wiley and Sons.

PRESS, H. W., TEUKOLSKY, S. A., VETTERLING, W. T. AND FLANNERY, B. P. (1992). *Numerical Recipes in FORTRAN.* Cambridge: Cambridge University Press.

SARPKAYA, T. (1975). Forces on cylinders and spheres in a sinusoidally oscillating flow. *J. appl. Mech.* **42**, 32–37.

SARPKAYA, T. AND ISAACSON, M. (1981). *Mechanics of Wave Forces on Offshore Structures.* New York: Van Nostrand-Reinhold.

SEYMOUR, R. J., TEGNER, M. J., DAYTON, P. K. AND PARNELL, P. E. (1989). Storm wave induced mortality of the giant kelp *Macrocystis pyrifera* in southern California. *Est. Coast Shelf Sci.* **28**, 277–292.

SPROTT, J. C. AND ROWLANDS, G. (1992). *Chaos Data Analyzer*. New York: American Institute of Physics.

SPRUGEL, D. G. (1983). Correcting for bias in log-transformed allometric equations. *Ecology* **64**, 209–210.

UTTER, B. D. AND DENNY, M. W. (1996). Wave-induced forces on the giant kelp *Macrocystis pyrifera* (Agardh): field test of a computational model. *J. exp. Biol.* **199**, 2645–2654.

WOLF, A., SWIFT, J. B., SWINNEY, H. L. AND VASTANO, J. A. (1985). Determining Lyapunov exponents from a time series. *Physica* D **16**, 285–317.

ZAR, J. H. (1974). *Biostatistical Analysis.* Englewood Cliffs, NJ: Prentice-Hall.